Materials Chemistry and Physics 148 (2014) 208–213

Contents lists available at ScienceDirect

Materials Chemistry and Physics

journal homepage: www.elsevier.com/locate/matchemphys

Synthesis, characterization and photocatalytic activity of WO_3/TiO_2 for NO removal under UV and visible light irradiation

E. Luévano-Hipólito [a], A. Martínez-de la Cruz [a, *], E. López-Cuellar [a], Q.L. Yu [b], H.J.H. Brouwers [b]

[a] CIIDIT, Facultad de Ingeniería Mecánica y Eléctrica, Universidad Autónoma de Nuevo León, Ciudad Universitaria, C.P. 66451 San Nicolás de los Garza, N.L., Mexico
[b] Department of the Built Environment, Eindhoven University of Technology, P.O. Box 513, 5600 MB Eindhoven, The Netherlands

HIGHLIGHTS

- WO_3/TiO_2 prepared in simple way show high photocatalytic activity for NO removal.
- The concrete was the best substrate to the performance of WO_3/TiO_2 with UV radiation.
- The glass was the best substrate to the performance of WO_3/TiO_2 with visible radiation.

GRAPHICAL ABSTRACT

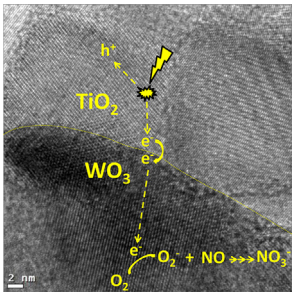

ARTICLE INFO

Article history:
Received 9 July 2013
Received in revised form
19 July 2014
Accepted 22 July 2014
Available online 15 August 2014

Keywords:
Oxides
Precipitation
Powder diffraction
Heterostructures

ABSTRACT

Samples with different proportions WO_3/TiO_2 were prepared by co-precipitation method followed by a heat treatment. The samples were characterized by X-ray powder diffraction (XRD), scanning electron microscopy (SEM), transmission electron microscopy (TEM), diffuse reflectance spectroscopy (DRS), and adsorption–desorption N_2 isotherms (BET). The photocatalytic properties of WO_3/TiO_2 samples were evaluated in the photo-oxidation reaction of nitric oxide (NO) under UV and visible light irradiation. The highest photocatalytic activity was observed in the WO_3/TiO_2 sample with a composition of 80% mole of TiO_2. Among the different substrates used for supporting the photocatalyst, the best results were reached over concrete and glass when it was exposed to UV and visible light irradiation, respectively. In overall, the photocatalytic efficiency of the synthesized materials was higher under UV than visible light irradiation.

1. Introduction

Nitrogen oxides (NO_x, NO + NO_2) emitted from stationary and mobile sources are the origin of various health and environmental problems, such as irritated eyes, headache, pulmonary emphysema, acid rain, acidification of aquatic systems, ozone depletion, and photochemical smog [1]. Due to high NO_x concentration usually observed along highways, efficient techniques for NO_x removal from the ambient environment are required. For this purpose, heterogeneous photocatalysis is a clean and non energy intensive technology to eliminate pollutants from the air [2–5].

When a semiconductor oxide is irradiated with an appropriate electromagnetic radiation, it is possible to induce a charge

* Corresponding author. Tel.: +52 (81) 83 29 40 20; fax: +52 (81) 83 32 09 04.
E-mail addresses: azael.martinezdl@uanl.edu.mx, azael70@yahoo.com.mx (A. Martínez-de la Cruz).

http://dx.doi.org/10.1016/j.matchemphys.2014.07.034
0254-0584/

separation in the semiconductor that produces free electrons (e^-) and holes (h^+) in its conduction (CB) and valence (CV) bands, respectively. If the charge pair is not recombined, both species can migrate separately to the semiconductor surface and then participate in oxidation (h^+) or reduction (e^-) reactions with chemical pollutants adsorbed on the surface of the semiconductor. Titanium dioxide (TiO_2) is one of the most important semiconductor photocatalysts used for such applications, owing to its chemical stability, cheapness, non toxicity, and structural stability [6,7]. However, TiO_2 has two main disadvantages. The first one is its wide energy band gap (3.2 eV for the anatase and 3.0 eV for the rutile) which limits the use of visible radiation from the solar spectrum. The second disadvantage is the rapid recombination of the photogenerated electrons and holes [8]. In this sense, several authors proposed different methods to avoid the electron–hole recombination and therefore enhance the efficiency of the photocatalytic process [9–11]. Among these methods, the combination of TiO_2 with other narrow band gap semiconductors provides an effective way to extend the lifetime of the photogenerated pair, leading to an increase in the efficiency of the photocatalyst.

Recently some novel photocatalysts based on heterostructures have been developed. For example, coupling TiO_2 with binary and ternary oxides such as $InVO_4$, $BiVO_4$, $FeVO_4$, Ag_3VO_4 [12], Bi_2O_3 [13], Bi_2MoO_6 [14] and WO_3 [15–17] have been reported. In the present work, the coupling of WO_3 (Eg = 2.6 eV) with TiO_2 (Eg = 3.2 eV) will be tested as photocatalyst in the NO photooxidation reaction. In addition, the influence of the nature of substrate, relative humidity and gas concentration on the photo-oxidation reaction performance will be investigated.

2. Experimental

2.1. Synthesis of WO_3/TiO_2 samples

All chemicals reagents were analytical grade and were used without further purification. Commercial TiO_2, AEROXIDE® P25 (80%anatase-20%rutile composition, specific surface area 50 $m^2\ g^{-1}$) was chosen as the reference photocatalyst. WO_3/TiO_2 samples were prepared using a coupling method. In a typical procedure, stoichiometric amounts of TiO_2 to get different molar percentages in $(1-x)WO_3/xTiO_2$ (x = 5%, 15%, 50%, 70%, 80%, and 87%) were dispersed under continuous stirring in 100 mL of HNO_3 (10% v/v). Then 0.00107 mol of ammonium tungstate hydrate ($H_{42}N_{10}O_{42}W_{12}\cdot H_2O$) (Aldrich, 99%) were added into the corresponding TiO_2 dispersion. The resulting suspension in each case was maintained under vigorous stirring for 1 h. Afterward, the suspension was put in repose for 1 day at room temperature (20 °C ± 1 °C). The aqueous solution was removed and the precipitate was dried at 100 °C in a hot plate for 1 day. The precipitate obtained for each composition was heated at 500 °C for 24 h in order to promote the formation of WO_3/TiO_2 samples with different molar percentages. The heat treatment was accompanied from the release of gases such as NH_3 and H_2O which come from by-products of reaction and from tungsten precursor decomposition. These samples will be identified hereafter as WTi5, WTi15, WTi50, WTi70, WTi80, and WTi87 where the number denotes the molar percentage of TiO_2 in the sample. For comparative purposes, WO_3 oxide was obtained by the same experimental procedure but without the addition of TiO_2.

2.2. Characterization

The structural characterization of WO_3/TiO_2 samples was carried out by X-ray powder diffraction using a D8 Advance diffractometer with Cu K_α radiation. Diffraction experiments were performed with a step size of 0.05° and a dwell time of 0.5 s. The morphology and particle size of the samples were analyzed by scanning electron microscopy (FEI Nova NanoSEM 200 with an accelerating voltage of 30 kV) and by transmission electron microscopy (JEOL 2010 instrument with an accelerating voltage of 200 kV), respectively. For SEM image analysis, 50 particles were used to estimate the particle size. The UV–Vis diffuse reflectance absorption spectra of the samples were obtained by using an UV–Vis spectrophotometer Perkin–Elmer Lambda 35 equipped with an integrating sphere. The BET surface area measurements were carried out by adsorption–desorption N_2 isotherms by means of a Bel-Japan Minisorp II surface area and pore size analyzer. The isotherms were evaluated at −196 °C after a pretreatment of the samples at 150 °C for 24 h.

2.3. Photocatalytic experiments

The photocatalytic activity of WO_3/TiO_2 samples was evaluated by the removal of nitric oxide from air under UV and visible light irradiation. The photocatalytic experiments were carried out in a laboratory test set-up designed according with the standard ISO 22197-1:2007 as shown in Fig. 1 [18]. The experimental setup consisted of a planar reactor cell, an UV or visible light source, a chemiluminescent NO_x analyzer, and a gas supply. Table 1 shows the main characteristics, dimensions and operating conditions of the system employed in the photocatalytic experiments. Three different building materials were selected as substrates of the photocatalysts tested: glass, concrete and wallpaper. The photocatalyst (0.4 g) was coated on the substrate in an area of 200 cm^2

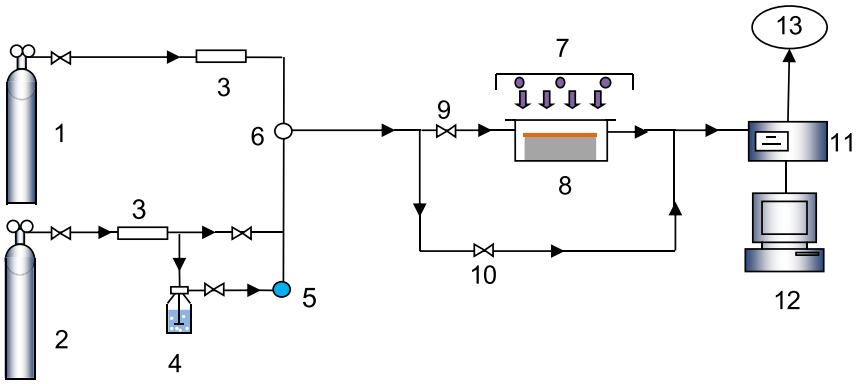

Fig. 1. Schematic diagram of the photocatalytic degradation set-up:1. NO gas supply; 2. Synthetic air; 3. Mass controller meter; 4. Humidifier; 5. Humidity controller; 6. Temperature and relative humidity sensor; 7. Light source; 8. Reactor; 9–10. Valve; 11. NO_x analyzer; 12. Computer; 13. Vent.

Table 1
Experimental set-up main characteristics and operating conditions.

Description	Operating conditions
Reactor	
Length (cm)	20
Width (cm)	10
Height (cm)	0.3
Volume (cm^3)	60
Substrate	
Length (cm)	20
Width (cm)	10
Light source	
Emission wavelength UV (nm)	300–400
Emission wavelength Vis (nm)	400–700
Flow rate (L min^{-1})	1
Irradiance flux (W m^{-2})	10
Relative humidity (%)	10–70
NO inlet concentration (ppm)	0.5–1

using colloidal silica as a binder. The coated materials were pre-treated at 100 °C in a ventilated oven to remove the free water from the suspension. Once the reactor was closed, the gas supply was started and the lamps were turned on in order to stabilize the radiation. After a short period (10 min), the adsorption–desorption equilibrium between gases and photocatalyst was achieved and the photocatalytic reaction was started. The NO_x concentration was continuously measured by a chemiluminescence NO_x analyzer (HORIBA APNA-370) with a sampling rate of 0.8 L min^{-1}. More detailed information about the test set-up and experimental procedure can be found elsewhere [19–21].

3. Results and discussion

3.1. Characterization

WO_3/TiO_2 samples were prepared by an aqueous method that involves the co-precipitation of chemical species containing Ti and W. The concentration of residual Ti ions in the solution removed from precipitates was analyzed by atomic absorption spectroscopy in order to determine an approximate final composition of TiO_2 in the samples. For all samples prepared, the analysis revealed a Ti ion concentration in solution less than 0.06 mg L^{-1} which represents, in general, a value near to 0.02% of the initial Ti added. On the basis of these results, it is possible to conclude that almost the total Ti added remained in the precipitate.

The nature of precipitate was not determined, because the material obtained was amorphous to XRD. In this point, the precipitate contains a mixture of phases coming from the TiO_2 dispersion and the paratungstate solution. The co-precipitation of both metal ions was carried out by different process. In the first case, when TiO_2 was dispersed in HNO_3, a semi-stable suspension was formed with the help of a continuous stirring. When the mechanical stirring was suppressed, a slow precipitation of TiO_2 took place. Due to this mechanical process, the size of particle decreases, producing an amorphous material. By the other hand, ammonium paratungstate was dissolved in acidic medium. Previous works have reported the behavior of the tungstate salt in aqueous media in presence of HNO_3 [22] and its precipitation, as is described by the follow equation:

$$(NH_4)W_{12}O_{41}\cdot 5H_2O + 10HNO_3 + 2H_2O \rightarrow 12WO_3\cdot H_2O + 10NH_4^+ + 10NO_3^-$$

where the tungsten oxide hydrate is separated from solution by precipitation after keeping the solution at rest for a day. According with the XRD, $WO_3\cdot H_2O$ was also amorphous. Then, the precipitate was formed by a contribution of TiO_2 and $WO_3.H_2O$ amorphous materials, which required an additional thermal treatment (500 °C) to crystallize.

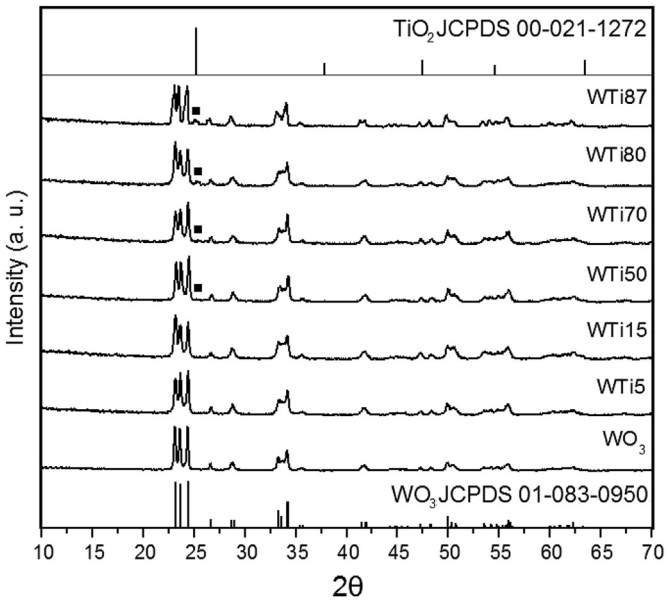

Fig. 2. XRD patterns of the WO_3/TiO_2 samples with different mole ratios of TiO_2. (■) TiO_2 anatase.

Fig. 2 shows the XRD patterns of samples with different WO_3/TiO_2 mole ratios. All diffraction lines were indexed with the monoclinic structure of WO_3 according to the JCPDS Card No. 01-083-0950, while diffraction lines of TiO_2 corresponding to anatase (JCPDS Card No. 00-021-1272) were observed only in samples WTi50, WTi70, WTi80 and WTi87. On the contrary, when the mole ratio of TiO_2 was low (5 and 15%), diffraction lines corresponding with TiO_2 were absent possibly due to the high dispersion of TiO_2 and its low concentration in these samples. Additional XRD experiments were performed in slower conditions (0.02 of step size with 1.5 s of dwell time) in order to detect the presence of diffraction lines of TiO_2 in samples with low concentration of this oxide (5 and 15%). Nevertheless the results were similar, and TiO_2 diffraction lines were no detected, as is showed in the supplementary figure. In addition, shift of the main diffraction lines of WO_3 was not observed after incorporating TiO_2, suggesting that the TiO_2 is located outside of the crystal structure of WO_3, without formation of solution solid between both phases.

The morphology of WO_3/TiO_2 samples with different TiO_2 mole ratios was examined by SEM. In general, as is shown in Fig. 3, TiO_2 particles were deposited on the surface of WO_3 (Fig. 3h). An elemental analysis by EDX revealed the identity of the TiO_2 particles dispersed on the WO_3 surface. As is shown in Fig. 3a, WO_3 in pure form is composed of particles with flake shape, but without the spherical aggregates on its surface associated with the presence of TiO_2 in the other samples. According to the images, TiO_2 particles appear gradually on the WO_3 surface as increasing its concentration in the WO_3/TiO_2 samples (Fig. 3b–h). Regardless of the TiO_2 mole ratio, flake-like particles were observed in all samples, which was consistent with the XRD results, indicating that TiO_2 is not incorporated in WO_3 structure. Table 2 shows the particle size of WO_3 estimated by SEM image analysis. With the increase of the TiO_2 mole ratio until 80%, the average particle size decreased from 320 to 180 nm. Nevertheless, at 87% some large particles of WO_3 were found, resulting in an increase of the particle size of the sample (see Fig. 3g).

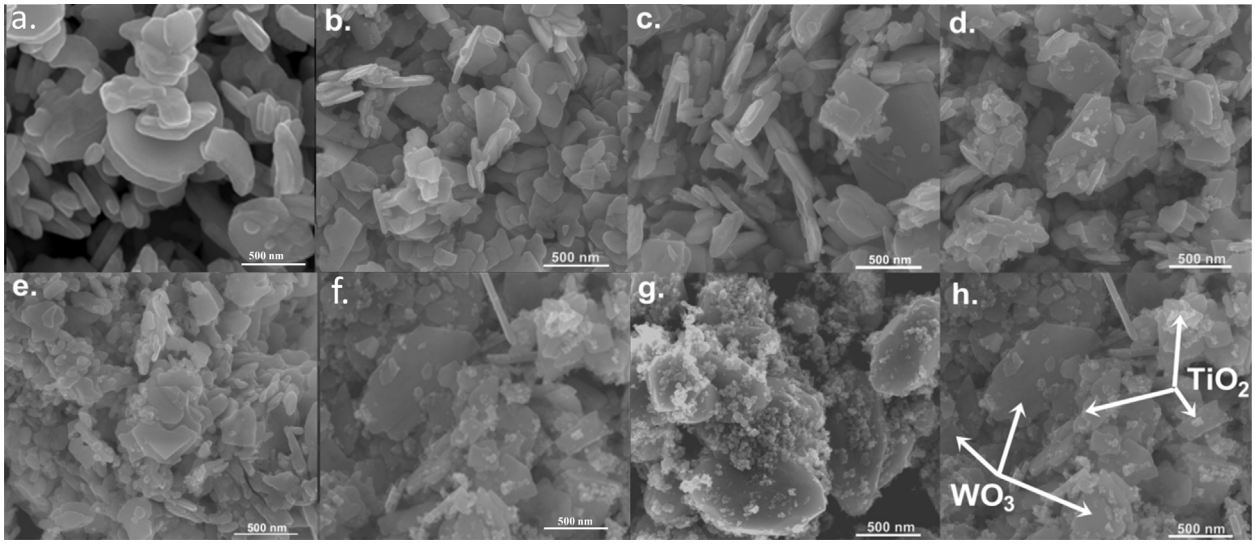

Fig. 3. SEM images of the as-prepared samples. a. 0% b. 5%, c. 15%, d. 50%, e. 70%, f. 80%, g. 87% TiO_2 mole and h. identification of WO_3 and TiO_2 particles in samples.

The micro-structure of WO_3/TiO_2 samples was analyzed by TEM and HRTEM. A typical TEM image at low magnification (Fig. 4a and b) of the sample WTi80 shows a flake-like morphology of the main phase with TiO_2 nanoparticles deposited on its surface, consistent with the SEM results. Further observation of the prepared sample by HRTEM (Fig. 4c) revealed the interface of the anatase structure of TiO_2 and monoclinic WO_3. Fig. 4c shows two types of clear lattice fringes. One set of fringes spacing is $d = 0.352$ nm, corresponding to the (101) crystallographic plane of anatase structure of TiO_2. Another set of fringes is $d = 0.364$ nm which corresponds to the (002) crystallographic plane of the monoclinic WO_3. In spite of the thermal treatment at 500 °C, the interface between WO_3 and TiO_2 particles was observed. This result suggests a heterojunction formed from these two oxides, which can be beneficial for improving the photocatalytic activity.

The BET surface areas of WO_3/TiO_2 samples are shown in Table 2. Specific surface areas of the pure oxides are 2.9 and 50 $m^2\ g^{-1}$ for WO_3 and TiO_2, respectively. When the TiO_2 mole ratio was increased, a slight increase in the surface area of WO_3/TiO_2 samples was observed from WTi5 to WTi50, and remained almost constant until WTi87. The UV–Vis diffuse-reflectance spectra of WO_3/TiO_2 samples showed that pure WO_3 oxide has an absorption edge of 485 nm with an estimated energy band gap of 2.5 eV, which is consistent with the literature [23,24]. As can be noticed in Table 2, WO_3/TiO_2 samples present similar energy band gaps values to WO_3. These values were ranging between 2.5 and 2.6 eV which corresponds with the typical value of WO_3. The absorption edge for the WO_3/TiO_2 samples indicated that TiO_2 can be activated in the visible region by combination with WO_3.

Table 2
Physical properties of the as-prepared samples with different TiO_2 mole ratio.

Sample	%mol TiO_2	Surface area BET ($m^2\ g^{-1}$)	Band gap (eV)	Particle size (nm)
WO_3	0	2.9	2.6	320
WTi5	5	5.5	2.5	320
WTi15	15	9.7	2.6	275
WTi50	50	12.3	2.6	270
WTi70	70	12.4	2.5	250
WTi80	80	13.3	2.6	180
WTi87	87	12.8	2.5	530

3.2. Photocatalytic activity

3.2.1. Effect of TiO_2 mole ratio on NO_x conversion

The photocatalytic activity of WO_3/TiO_2 samples with different TiO_2 mole ratios was evaluated by the removal of nitric oxide (NO) in gas phase under both UV and visible light irradiation. Fig. 5 shows the NO conversion (%) as a function of TiO_2 mole ratio supported over glass. Compared with WO_3 pure, the WO_3/TiO_2 samples showed higher photocatalytic activity towards the NO conversion under both UV and visible light irradiation. However, at low TiO_2 mole ratio (5%) the NO conversion was only 30% and 8% compared with observed for higher TiO_2 mole ratios (>80%) under UV and visible light irradiation, respectively. These results indicate that the introduction of TiO_2 on the WO_3 surface enhances the photocatalytic activity of WO_3, possibly by promoting the separation of photogenerated electrons and holes, as a result of the heterostructure formation. The samples WTi70 and WTi80 exhibited the highest NO conversion under UV and visible light irradiation, respectively. At the highest TiO_2 mole ratio (WTi87), the large particle size observed could have a negative effect on the photocatalytic process. For this sample, there could be a high concentration of recombination charge centers in the travel followed by holes and electrons from its generation point to the photocatalyst surface. In the latter process, the photogenerated electrons and holes will recombine, decreasing the photocatalytic activity.

3.2.2. Effect of substrate on NO_x conversion

Different substrates typically used as building materials such as concrete, glass and wallpaper were chosen to investigate the effect of substrate on NO conversion. As is shown in Fig. 6, when WTi80 was used as photocatalyst, the highest NO conversion was reached when concrete and glass were used as substrates under UV and visible light irradiation, respectively. Less satisfactory results were obtained for the wallpaper sample, where only 36% (UV) and 6% (Vis) of NO was removed. As can be seen from Fig. 6, when concrete was used as substrate under UV light irradiation, NO_2 was not observed as a product of the reaction, suggesting that NO was fully oxidized to NO_3^- [25,26]. These generated nitrate ions are deposited on concrete surface but due to its high surface area, the deactivation of the photocatalyst was not observed. In the case of wallpaper, with the lowest NO conversion, <2% of the NO removed was oxidized to NO_2 under both UV and Visible light irradiation.

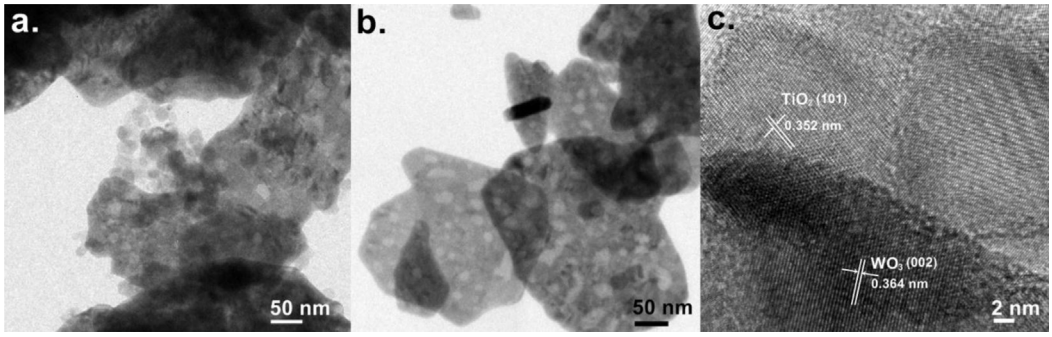

Fig. 4. TEM and HRTEM images of WO_3/TiO_2 sample: a, b. TEM and c. HRTEM image.

Assuming a complete oxidation from NO to NO_3^- ion, deposition of nitrate ions over the surface of wallpaper could occupy the adsorptive sites and prevent the contact between the NO molecules and WO_3/TiO_2 surface, leading to the deactivation of the photocatalyst. Finally, when glass was used as substrate the NO_2 formation was around 20% of the NO removed. The photocatalyst deactivation under both UV and Visible light irradiation as reported in the literature for similar materials and experimental conditions [27,28]. The NO conversion (%) using different substrates under UV irradiation increased in the following order: Concrete > Glass > Wallpaper, and with visible light irradiation it follows the order: Glass > Concrete > Wallpaper.

3.2.3. *Effect of relative humidity on NO_x conversion*

The effect of relative humidity on the photocatalytic removal of NO is observed in Fig. 7. The experiments were carried out with the sample WTi80 supported over concrete under UV light irradiation. The results show a high NO removal from air with the different samples used as photocatalyst. In fact, NO conversion (%) was almost constant and decreased only slightly with increasing the relative humidity from 10 to 70%. These data revealed that the degradation of NO to NO_2 is not conditioned by the presence of water vapor in the air. Nevertheless, in this range of relative humidity, final NO_2 concentration showed important differences in relation with the relative humidity, i.e., 0, 11, 23, and 26% for 10, 30, 50, and 70% of RH. This situation can be associated with the different rates of reactions for NO_2 formation and NO_2 degradation in each sample by the presence of humidity. The formation of NO_2 seems not be affected by the humidity level (assuming a direct reaction from NO to NO_2), but humidity level can be the factor that rules the rate conversion of NO_2 to NO_3^- ions. An analysis of NO_x seems to confirm this point. As can be seen in Fig. 7, the optimal value of relative humidity is 10%. At this value, the highest NO_x conversion was reached and NO_2 gas as intermediate product was not observed as product of the photocatalytic reaction. From this result is possible to conclude that under these experimental conditions, 94% of NO_x ($NO + NO_2$) was oxidized into NO_3^- as the final product. The decrease in the photocatalytic efficiency as the relative humidity increases from 10 to 70% can be explained by the competition of adsorption sites of the WO_3/TiO_2 surface between NO_2 and H_2O molecules.

3.2.4. *Effect of inlet NO concentration on NO_x conversion*

Additional experiments were done in order to investigate the effect of inlet NO concentration in the NO_x ($NO + NO_2$) conversion using the sample WTi80 supported over concrete at 10% RH under UV light irradiation. Fig. 8 shows that NO conversion remains constant (94%) as inlet concentration increases from 0.5 to 1 ppm. The NO_2 formation (%) from NO removed slightly increases until 5% when 1 ppm was used as inlet NO concentration. The NO_x ($NO + NO_2$) conversion was 94%, 92% and 89% for 0.5, 0.7, and 1 ppm, respectively of the initial concentration of NO.

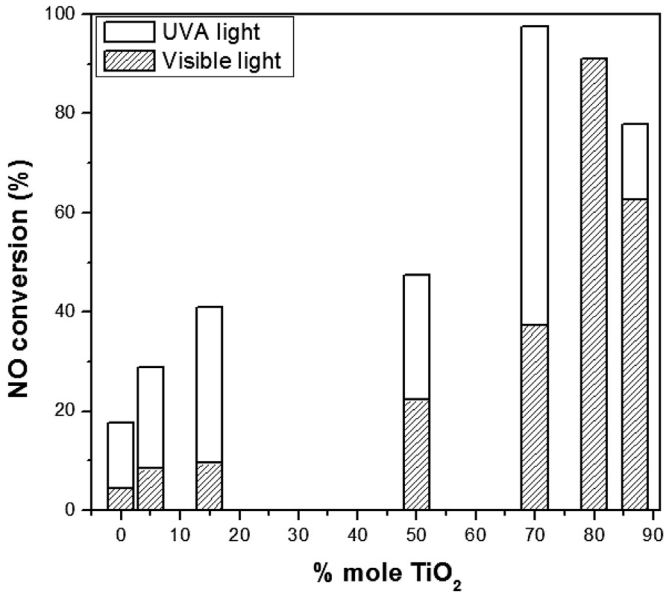

Fig. 5. NO conversion (%) as a function of TiO_2 mole ratio using WO_3/TiO_2 heterostructures as photocatalysts supported over glass under UV and Visible light irradiation. ($\tau_R = 3.6$ s, HR = 50%, $E = 10$ W m^{-2}, 1% of error in measurements).

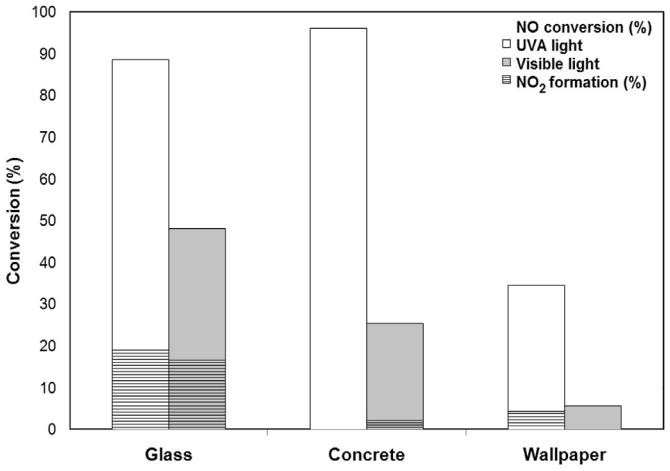

Fig. 6. Substrate effect in NO_x conversion (%) using WO_3/TiO_2 as photocatalyst under UV and visible light irradiation. ($Q = 1$ L min^{-1}, RH = 10%, $E = 10$ W m^{-2}, 1% of error in measurements).

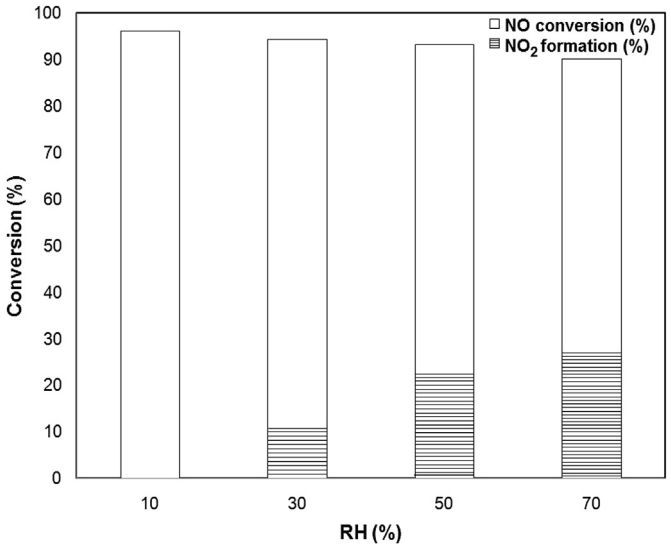

Fig. 7. Humidity effect in NO_x conversion (%) using WO_3/TiO_2 as photocatalyst supported over concrete under UV light irradiation. ($Q = 1$ L min^{-1}, $E = 10$ W m^{-2}, 1% of error in measurements).

Based on the above results, WO_3/TiO_2 samples exhibited enhanced photocatalytic activity under UV and visible light irradiation. This situation can be explained due to the interaction between WO_3 and TiO_2, which involves an electron transfer. Since the conduction band (CB) of WO_3 has a potential more positive than the CB of the TiO_2, the photogenerated electrons from TiO_2 can be transfer to the CB of WO_3 under UV light. This electron transfer leads to an increase in the lifetime of the photogenerated electrons and holes and as a consequence to a promotion in the efficiency of the photocatalytic oxidation of NO. On the other hand, under visible light irradiation only WO_3 is excited (2.6 eV). The increase in the photocatalytic activity of WO_3/TiO_2 samples under visible light irradiation can be attributed to the synergistic effect between both oxides, in which NO molecules are adsorbed on the TiO_2 surface to be able to react with the photogenerated electrons and holes formed in WO_3. In this sense, the sample with the highest photocatalytic activity under visible light irradiation (WTi80) also has the lowest particle size, thereby allowing the transport of photogenerated electrons and holes to the surface to be able to react with NO adsorbed on the TiO_2 surface. From these results, WO_3/TiO_2 sample with 80% mole of TiO_2 in its composition can be considered as an efficient photocatalyst to remove NO from air under UV and visible light irradiation.

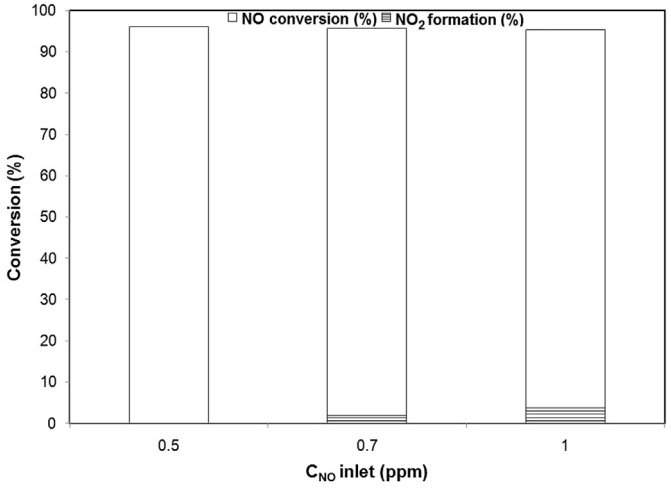

Fig. 8. Inlet NO concentration in NO_x conversion (%) using WO_3/TiO_2 as photocatalyst supported over concrete under UV light irradiation. ($Q = 1$ L min^{-1}, $E = 10$ W m^{-2}, 10% RH, 1% of error in measurements).

4. Conclusions

WO_3/TiO_2 heterostructures consisting of monoclinic WO_3 and anatase TiO_2 crystalline phases were prepared by a co-precipitation and calcination method. It was found that the optimal content of TiO_2 in WO_3/TiO_2 heterostructures in NO conversion was 70 and 80% mole for UV and visible light irradiation, respectively. On the other hand, when concrete was used as substrate an increase in NO conversion was observed under UV light irradiation due to its higher surface area to absorb more NO molecules compared to glass and wallpaper. The efficiency in NO conversion is affected by increasing the relative humidity in terms of the NO_2 formed, the optimal level was 10% with a minimum of NO_2 generated using concrete as substrate under UV light irradiation. The inlet NO concentration has not a significant effect in NO conversion under the same conditions.

Appendix A. Supplementary data

Supplementary data related to this article can be found at http://dx.doi.org/10.1016/j.matchemphys.2014.07.034.

References

[1] C.J. Pereira, M.D. Amidiris, ACS Symp. Ser. 587 (1995) 1–13.
[2] J. Zhang, Y. Hu, M. Matsuoka, H. Yamashita, M. Minagawa, H. Hidaka, M. Anpo, J. Phys. Chem. B 105 (2001) 8395–8398.
[3] K. Demeestre, J. Dewulf, B. De Witte, A. Beeldens, H. Van Langenhove, Build. Environ. 43 (2008) 406–414.
[4] R. Portela, B. Sánchez, J.M. Coronado, R. Candal, S. Suárez, Catal. Today 129 (2007) 223–230.
[5] C.H. Ao, S.C. Lee, J.C. Yu, J. Photochem. Photobiol. A Chem. 156 (2003) 171–177.
[6] A.L. Linsebigler, G. Lu, J.T. Yates, Chem. Rev. 95 (1995) 735–758.
[7] A. Fujishima, T.N. Rao, D.A. Tryk, J. Photochem. Photobiol. C Photochem. Rev. 1 (2000) 1–21.
[8] M. Ni, M.K.H. Leung, D.Y.C. Leung, K. Sumathy, Renew. Sustain. Energy Rev. 11 (2007) 401–425.
[9] D.K. Lee, I. Cho, S. Lee, S. Bae, J.H. Noh, D.W. Kim, K.S. Hong, Mater. Chem. Phys. 119 (2010) 106–111.
[10] T.T. Le, M.S. Akhtar, D.M. Park, J.C. Lee, O. Yang, Appl. Catal. B Environ. 111–112 (2012) 397–401.
[11] Z.L. Zhang, M. Wan, Y.L. Mao, J. Photochem. Photobiol. A Chem. 233 (2012) 15–19.
[12] Y. Min, K. Zhang, Y. Chen, Y. Zhang, Chem. Eng. J. 175 (2011) 76–83.
[13] J. Zhu, S. Wang, J. Wang, D. Zhang, H. Li, Appl. Catal. B Environ. 102 (2011) 120–125.
[14] N. Li, L. Zhu, W. Zhang, Y. Yu, W. Zhang, M. Hou, J. Alloys Compd. 509 (2011) 9770–9775.
[15] V. Iliev, D. Tomova, S. Rakovsky, A. Eliyas, G. Li Puma, J. Mol. Catal. A Chem. 327 (2010) 51–57.
[16] Y. Li, L. Chen, Y. Guo, X. Sun, Y. Wei, Chem. Eng. J. 181–182 (2012) 734–739.
[17] F. Wang, X. Chen, X. Hu, K.S. Wong, J.C. Yu, Sep. Purif. Technol. 91 (2012) 67–72.
[18] Q.L. Yu, PhD Thesis, University of Technology, Eindhoven, The Netherlands (, 2012, pp. 111–143.
[19] Q.L. Yu, H.J.H. Brouwers, Appl. Catal. B Environ. 92 (2009) 454–461.
[20] G. Hüsken, M. Hunger, H.J.H. Brouwers, Build. Environ. 44 (2009) 2463–2474.
[21] M.M. Ballari, M. Hunger, G. Hüsken, H.J.H. Brouwers, Appl. Catal. B Environ. 95 (2010) 245–254.
[22] S. Supothina, P. Seeharaj, S. Yoriya, M. Sriyudthsak, Ceram. Int. 33 (2007) 931–936.
[23] A. Martínez-de la Cruz, D. Sánchez Martínez, E. López Cuellar, Solid State Sci. 12 (2010) 88–94.
[24] D. Chen, H. Wang, R. Zhang, L. Gao, Y. Sugahara, A. Yasumori, J. Ceram. Process. Res. 9 (2008) 596–600.
[25] J.C. Jung, H. Lee, H. Kim, Y. Chung, T.J. Kim, S.J. Lee, S. Oh, Y.S. Kim, I.K. Song, J. Mol. Catal. A Chem. 271 (2007) 261–265.
[26] T. Ibusuki, K. Takeuchi, J. Mol. Catal. 88 (1994) 93–102.
[27] C.L. Bianchi, C. Pirola, E. Selli, S. Biella, J. Hazard. Mater. 211 (2012) 203–207.
[28] T. Martinez, A. Bertron, E. Ringot, G. Escadeillas, Build. Environ. 46 (2011) 1808–1816.